Experimental realization of a pillared metasurface for flexural wave focusing

Wan Wang[1,#], Julio Iglesias[2,#], Yabin Jin[1,*], Bahram Djafari-Rouhani[3], Abdelkrim Khelif[2,*]

[1]School of Aerospace Engineering and Applied Mechanics, Tongji University, 200092 Shanghai, China

[2]Institut FEMTO-ST, CNRS, Université de Bourgogne Franche-Comté 15B Avenue des Montboucons, CEDEX, F-25030 Besançon, France

[3]Institut d'Electronique, de Microélectonique et de Nanotechnologie, UMR CNRS 8520, Département de Physique, Université de Lille, 59650 Villeneuve d'Ascq, France

[#]Equal contribution

[*]Corresponding author: 083623jinyabin@tongji.edu.cn; abdelkrim.khelif@femto-st.fr

Abstract

A metasurface is an array of subwavelength units with modulated wave responses that show great potential for the control of refractive/reflective properties in compact functional devices. In this work, we propose an elastic metasurface consisting of a line of pillars with a gradient in their heights, erected on a homogeneous plate. The change in the resonant frequencies associated with the height gradient allows to achieve transmitted phase response covering 2π range while the amplitude response remaining at a relatively high level. We employ the pillared units to design focusing metasurface and compare the properties of the focal spots through simulation and experiment. Subwavelength transverse and lateral full width at half maximum (FWHM) of the focusing intensity profiles are observed in both simulation and experiment with the underlying mechanism being the interference and diffraction of the scattered waves from the resonant pillars as well as the boundaries (especially for experiment). The good correspondence between the experimental and simulated relative focal length shows the robustness of the focusing pillared metasurfaces with respect to fabrication imperfections. This proposed compact, simple and robust metasurface with unaffected mechanical properties provides a new platform to elastic wave manipulation for energy harvesting, wave communication, sensing, non-destructive testing, among others.

Keywords: elastic metasurface; focusing; robustness; Lamb wave; generalized Snell's law

1. Introduction

A metasurface consists of an array of subwavelength thickness units exhibiting inhomogeneous or modulated phase response that can arbitrarily manipulate refracted or reflected wavefronts. This field was rapidly developed in the domains of optics [1-5], microwave [6-8], and acoustics [9-18]. Recently it has been extended to elastic waves [19-21] especially for Lamb waves in plates with diverse potential applications at different scales. The key feature to design an elastic metasurface is to realize a 2π phase span response by the constituting units while keeping a relative high level of the wave amplitude. As known by the classical wave motions, the propagating speeds of the Lamb waves depend on the elastic properties of the host medium and the plate's thickness (for flexural mode)[22, 23]. A large number of works focus on tailoring the plates to design composite in-plane geometries in order to fulfill the 2π phase shift span requirement[24-34]. Although in-plane geometries provide a wide platform to manipulate wave responses with different mechanisms, they will significantly reduce the stiffness of plates which is very important as concerns the mechanical property of the structure.

An alternative solution is to design added out-of-plane units on the plate, for instance, by adding a thin patch with a size of the order of the wavelength for reflected wave response[35], or a set of slender pillars with a subwavelength total length for transmitted wave response[36, 37]. Given that a pillar is able to exhibit rich resonant properties[38-43], one can take advantage of the phase shift around the resonance to build the units of the array in the metasurface. For example, a set of graded pillars can produce different phase shifts in their transmission coefficient. However, in general, the variation of the phase around a resonance span a region of π instead of 2π. In ref. [38], some of the authors showed that the phase shift can cover a range of 2π if we superpose at the same frequency the fundamental compressional mode of the pillar with one of its bending modes. Based on this result, ref. [44] proposed theoretically the design of a metasurface, constituted by a set of pillars with graded heights, to achieve subwavelength focusing and imaging of flexural Lamb waves. The purpose of the present paper is the first experimental realization of such a design.

In this work, we experimentally realize a pillared metasurface consisting of a transverse line of graded height resonant pillars with identical subwavelength diameter that is able to design various wavefront functions. Each pillar of the metasurface acts as a secondary excitation source with different transmitted phases through the interference between the incident wave and the re-emitted wave. It is found that the transmitted phase response covers 2π shift while the amplitude remains at sufficiently high level. In Sec.2, we present the design process of the metasurface unit for phase and amplitude manipulation which is further adopted to design plane wave focusing effect. In Sec.3, we fabricate the pillared metasurface and experimentally demonstrate focusing effect in good comparison with the numerically predicted results. Finally, we make a summary of this work in section 4.

2. Pillared metasurface design

We first consider the transmission through a line of identical pillars arranged on the plate in the frequency domain, as shown in Fig.1(a). Periodic conditions are applied on the two sides of the unit cell along the x direction to simulate the infinite line of uniform pillars. Perfect matching layers (PML) are also applied to the two ends of the unit cell along y direction to avoid wave reflections from the edges. An incident plane flexural wave (the dominant component is the out of plane displacement) source is excited by an out of plane face force, and the transmitted wave is detected at a point on the plate's surface after the pillar. By analyzing the wavenumber of the transmitted wave with Fourier transformation method, it is found that the transmitted wave is still dominated by the flexural wave, as seen the appendix for details. The transmission coefficient is defined as

$$T = \left|\frac{w_0}{w_{\text{ref}}}\right|$$

where w_0 and w_{ref} are the out-of-plane displacement of the detection point with and without the pillar respectively. Generally, two types of resonant modes, namely bending and compressional modes, can be excited by the incident plane wave; then the pillars play as a secondary source and emit out-of-phase scattering wave. The transmitted wave results from the interference between the incident and re-emitted waves[38]. For a specific case, the bending and compressional modes can occur at the same frequency to enhance the re-emitting effect, making the amplitude of the scattering wave as about 1.55 times that of the incident wave. After the destructive interference of the scattering and the incident waves, the transmitted wave is dominated by the scattering wave, with an out-of-phase transmission coefficient of amplitude 0.55.

We set the pillar's diameter d = 3.6 mm, pillar's height h = 6.6 mm, plate thickness e = 6.0 mm, unit width w = 4.8 mm. The pillar and plate are made of 3D-printed materials polylactic acid (PLA) with Young's modulus E as 3.5GPa, Poisson's ratio as 0.36 and density as 1240 kg/m^3 (provided from the manufacturer). The above parameters are chosen appropriately such that the superposition effect of the bending mode and compressional mode can be achieved at 59.2 kHz corresponding to the simulated wavelength λ = 13.3 mm. The diameter of the pillar is only 0.27λ, being deep subwavelength. It should be mentioned that the size of the pillars can be scaled up and down to drive the working frequency to lower or higher range, respectively.

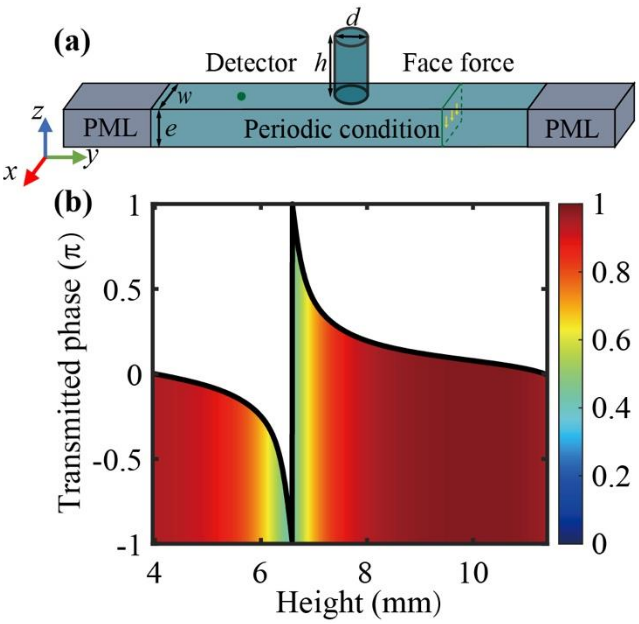

FIG. 1. (a) Illustration of the pillared metasurface unit. The flexural wave is excited by the out of plane face force and detected at a point on the plate's surface after the pillar. Periodic conditions are applied to the two boundaried along x direction. The cyan area represents PLA materials, and

the dark gray areas are the perfect matched layers. (b) Transmitted phase (black curve) and amplitude (color level) as a function of the pillar height h in the metasurface unit.

By sweeping the pillar's height at 59.2 kHz while maintaining other parameters as mentioned above, Fig. 1(b) shows the transmitted amplitude and phase responses of the displacement u_z. It is found that when the pillar's height is swept from 4 mm to 11.4 mm, the transmitted phase can fully cover the range from -π to π, as shown by the black curve, and the transmitted amplitude keeps a relatively high level, as shown by the color map. Then it is possible to manipulate the transmitted wavefront based on the generalized Snell's law for various advanced functions, such as beam deflection, focusing, source illusion, wave suppression, among others. Focusing is one of the widest effects studied in wave physics, which is widely used in non-destructive testing or signal reception as for sensing application[45]. Therefore, we select it to demonstrate the functionality of the proposed pillared metasurface. To design a plane wave focusing effect, it requires a gradient phase response along the transverse x axis in the metasurface. The continuous phase response profile $\varphi(x)$ can be given as

$$\varphi(x) = \frac{2\pi}{\lambda}\left(\sqrt{F^2 + x^2} - F\right) + \varphi(x = 0) \qquad \text{Eq. (1)}$$

where F and x are the focal length and x-coordinate position along the metasurface, respectively, λ is the working wavelength. Since the real metasurface is made up of individual pillars and cannot represent continuous phase shift, the continuous phase profile needs to be discretized into the required phase points according to pillar's positions along the metasurface. In Fig. 2(a), we calculate the continuous phase profile (blue curve) by Eq. (1) for the plane wave focusing with a focal length F=λ, and discretize it into 31 phase points (orange dots) for a pillared metasurface composed of 31 pillars. The number of pillars is limited by the maximum size capacity of 3D printer. The phase of the central unit is set as -π, corresponding to the strongest resonant status of the pillar. However, it should be noted that the choice of the central phase is not the key factor for the focusing effect, and other phases can be set as well. Once the discrete phases of metasurface units are obtained, the corresponding pillar' heights can be easily retrieved from the black curve in Fig. 1(b). The final designed metasurface composed of 31 gradient pillars is shown in Fig.2(b).

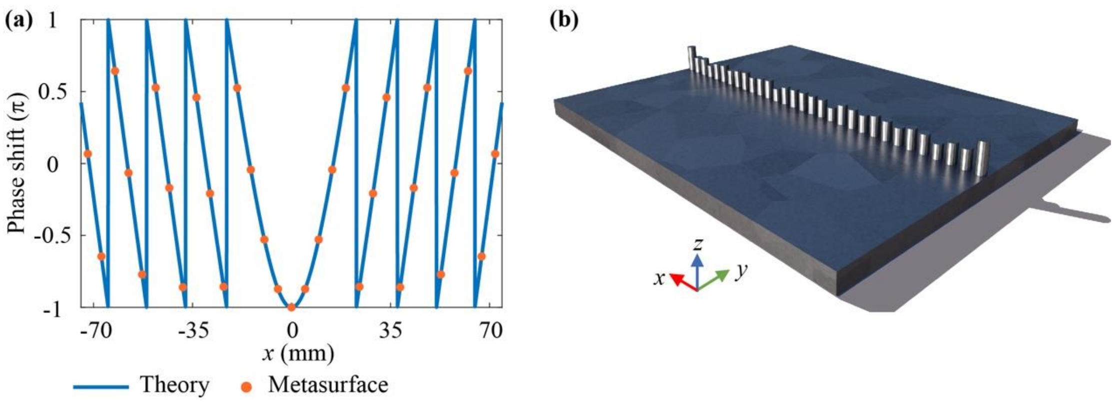

FIG. 2. (a) Theoretical phase profile (blue line) and discrete phases (orange dots) of the 31 pillars metasurface along *x* axis with the designed focal length $F=\lambda$. (b) Illustration of the designed pillared metasurface.

3. Numerical and Experimental demonstrations of focusing effect

A focusing metasurface containing 31 pillars with the focal length as $F=\lambda$ is consequently designed as shown in Fig. 3(a). To launch the incident wave, we followed a process close to the experiment. Namely, three piezoelectric ceramic transducers PZT patches with dimension of 2.58 mm thick, 50 mm length and 10 mm width, as the dark green area shown in Fig. 3(a), are arranged on the upper surface of the plate to excite flexural waves by applying an electric field of amplitude of 10V between the electrodes. The PZT patch made of lead zirconate titanate have the followings material properties with piezoelectric constants $e_{31} = e_{32} = -5.2$ C m^{-2}; dielectric permittivity $\varepsilon_{33}=663.2\ \varepsilon_0$, with ε_0 being the vacuum permittivity. We fabricate the sample with PLA material for experiment by using 3D printing technology and its picture is presented in Fig.3(b). The three identical PZT patches are glued to the upper surface of the plate for exciting flexural waves, as shown by the yellow stripe in Fig. 3(b); the patches are driven with a signal at the frequency of 59.2kHz and an electric amplitude of 10V. The out of plane displacement is measured with a Doppler laser vibrometer, MSA-500 by polytec supplied by analog displacement decoder model DD-300 with sensitivity of 50nmV^{-1}. The interested area of the focusing field is chosen as a square purple zone, $L_1 = L_2 = 30$ mm, and further divided in rectangular subsections which is as big as the field of view of the objective with size 3.5 mm by 4.5 mm. The displacement is scanned along *x*-*y* plane with a step of 335μm in each subsection. Absorbing materials are applied to the surrounding of the sample during the experimental measurement in order to reduce the boundary reflecting effect as much as possible.

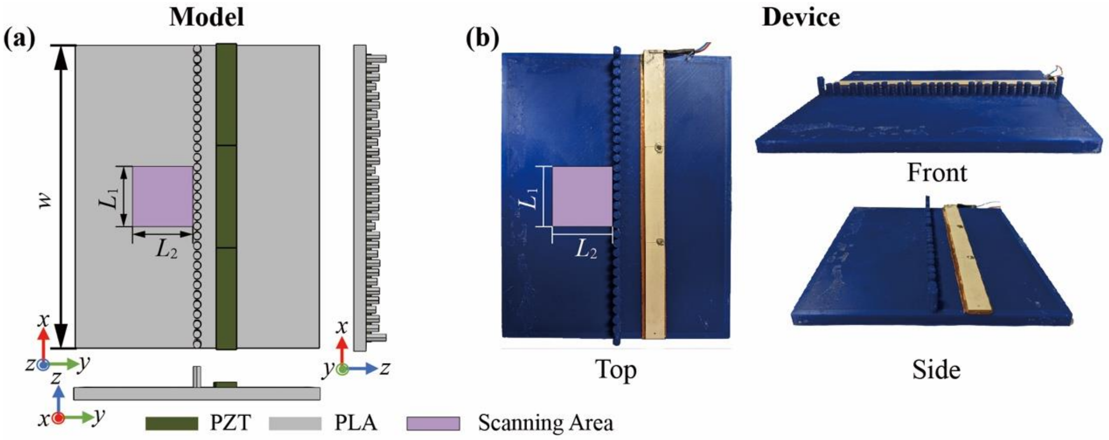

FIG. 3. Illustration of the simulating geometric model (a) and the experimental device (b). The scanning area is also shown as purple color.

We present the simulated (E=3.5 GPa) and experimental results of the focusing effect in Fig.4(a) and (c). A clear focusing spot is observed with both approaches, supporting the focusing functionality of the pillared metasurface. The simulated focal length is found to be 19.9mm corresponding to 1.50λ, since the wavelength of the flexural Lamb wave is λ=13.3mm as mentioned in the previous section. In the experiment, the wavelength of the Lamb wave is found to be 15.2mm and the measured focal length is 22.6mm corresponding to1.48λ. Therefore, the two focal lengths are very close to each other when expressed in units of the wavelength, while they show 15% deviation in their absolute values. We infer this to a deviation of the Young's modulus *E*' of the actual 3D printed sample as compared to the value *E* provided by the manufacturer. To make a more quantitative comparison with experiment, we simulated the behavior of the fabricated sample at the same frequency of 59.2kHz with a Young's modulus of *E*'=5 GPa that reproduces the experimental wavelength. The result is shown in Fig.4(b) where one can note a focal length of 22.0 mm (corresponding to 1.45λ), in good agreement with experiment. Additionally, the new simulation reproduces well the two experimental hot spots in the close vicinity of the metasurface, at the level of the two pillars on both sides of the central pillar. However, caution should be taken that with the new value *E'* of the Young's modulus, the pillars in the fabricated sample no longer satisfy the exact phase shift conditions chosen from Fig. 2 during the initial design process. Another difference between the experimental results and the simulations is about the asymmetry of the measured pattern. We think that this can be attributed to some fabrication and experimental imperfections that will be mentioned below.

For a more quantitative comparison, we compare the size of the simulated and experimental focal spots in terms of their corresponding wavelengths, Fig. 4(d) and (e) display the intensity profile along the *x* and *y* directions crossing the focal spot, respectively. For simulated (*E*=3.5 GPa) case, the full width at half maximum (FWHMs) obtained from the intensity field along *x* and *y* axes are 0.46λ and 0.99λ, respectively, as shown by the brown curves. The FWHM along *x* axis in simulation is subwavelength, originating from the interference and diffraction of the gradient secondary sources[11, 44, 46]. For simulated (*E*'=5 GPa) case, the FWHMs along *x* and *y* axes become 0.90λ and 0.91λ, respectively, as shown by the green curves. One can note that we lose the subwavelength FWHM along x which can be explained by the deviation of the actual pillars from an accurate design based on the correct value *E'* of the Young's modulus. For the experimental case, the FWHMs along *x* and *y* axes are 0.78λ and 0.39λ, respectively, as shown by the blue curves in Fig. 4(d) and (e). The FWHM along x is also above λ/2 and qualitatively close to the second simulation. As concerns the experimental FWHM along y, it has a complicated shape due to the asymmetry of the whole transmission pattern. This asymmetry may result from different imperfections in the sample or possibly in the experimental excitation of the incident wave, in particular the lateral boundary conditions and the induced reflection in the experimental configuration, the fabrication imperfections and the gluing, the bandwidth of the transducers, the proximity of the transducers to the sample which can generate an imperfect plane wave.

From the above discussion, one can conclude that the focusing effect is observed in all the three above approaches and the relative focal lengths in terms of corresponding wavelength are very close to each other. This indicates a robust focusing property of the metasurface despite the actual differences between the experiment and simulation. It is further expected that if the ratio between the focal length and the metasurface length decreases, one can achieve a deep sub-diffraction focusing effect with the transverse FWHM much smaller than half a wavelength, and the focusing effect can be robustly conserved over a certain frequency range [44].

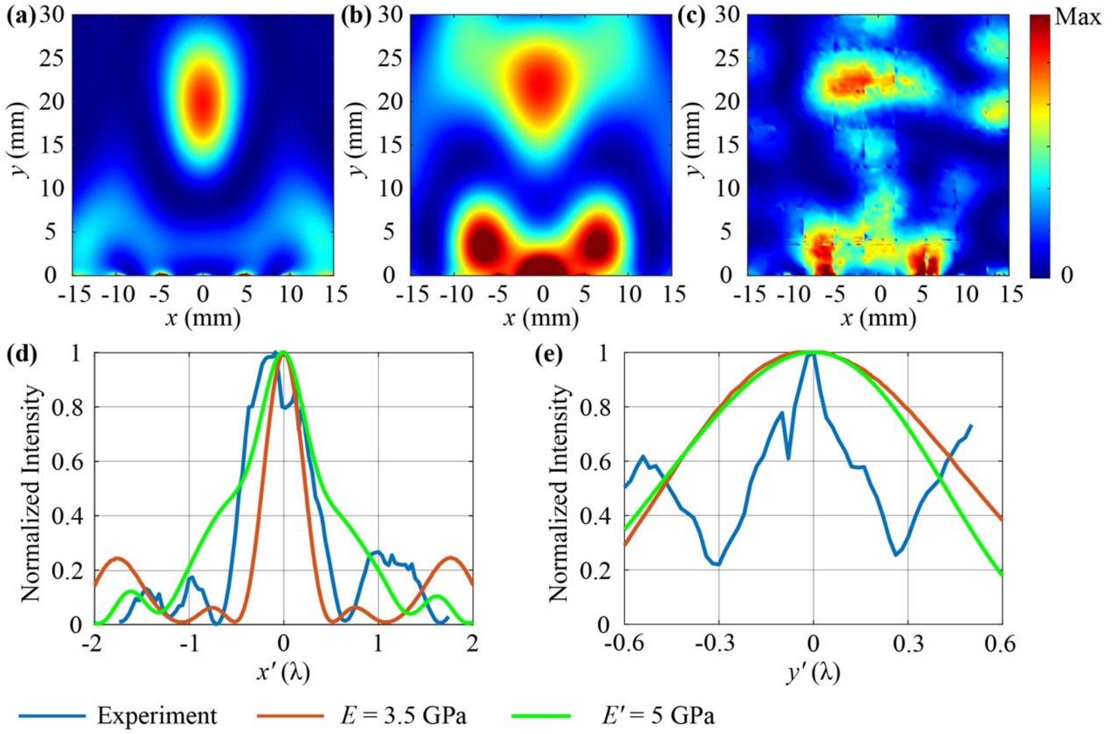

FIG. 4. Intensity fields of the scanning area of focusing effect obtained by simulation with (a) E=3.5 GPa, (b) E'=5 GPa and (c) experiment. Intensity profiles along the x axis (d) or y axis (e) crossing the focusing point. Brown, green and blue curves represent results from simulation with E=3.5 GPa, E'=5 GPa and experiment, respectively. x' and y' are local coordinate systems with the focal point as the origin.

4. Conclusion

In summary, we numerically and experimentally demonstrated a pillared metasurface, consisting of a line of pillars with gradient heights, for focusing an incident plane flexural wave into a spot. We took the advantage of the superposition of the bending and compressional modes of the pillar on a homogeneous plate which is able to enhance the out-of-plane scattering wave with the amplitude larger than that of the incident wave. After the destructive interference between the scattering and incident waves, the transmitted wave is out of phase. The phase response of the pillared units spans a 2π shift range and the amplitude response keeps at a relatively high level. We designed and fabricated a focusing metasurface, and compared the measured focusing spots quantitatively with simulations. The FWHM along x for simulated spot is subwavelength due to the interference and diffraction of the re-emitted waves in the near field. The experimental and simulated relative focusing lengths have a good agreement, showing a strong robustness of the focusing metasurface. This metasurface can also be extended to surface waves, such as Rayleigh waves [47]. The simple, compact and robust design of the proposed pillared metasurfaces without tailoring the plate open a new avenue for advanced elastic wave functions in great potential applications for MEMS, civil engineering, aerospace engineering, marine engineering, and so on.

Acknowledgment

This work was supported by the National Natural Science Foundation of China (Grant No. 11902223), the Shanghai Pujiang Program (Grant No. 19PJ1410100), the program for professor of special appointment (Eastern Scholar) at Shanghai Institutions of Higher Learning, the Fundamental Research Funds for the Central Universities, and the High-Level Foreign expert Program. This work is also partially supported by the French EIPHI Graduate School (contract "ANR-17-EURE-0002").

Data Availability

The data that support the findings of this study are available from the corresponding author upon reasonable request.

Appendix. Mode analysis

In Fig.5(a), the out of plane displacements in the 'Object area' are selected to perform the Fast Fourier Transformation (FFT) to analyze the wavenumber of transmitted waves. First, both flexural/antisymmetric (black) and symmetryc (blue) Lamb modes incident waves are independently excited in the bare plate without the pillars. The positions of the black and blue intensity peaks correspond to the wavenumber values of the antisymmetric and symmetryc Lamb modes, respectively. Then we excite the antisymmetric Lamb wave in the plate with the pillars, the intensity is plotted as the dotted red line. It is found that there are two peaks occurred at the wavenumbers of the antisymmetric and symmetric Lamb modes. The intensity value of the antisymmetric Lamb mode is over one magnitude bigger than that of the symmetric Lamb mode, supporting that the transmitted waves after the pillars are dominated by the flexural/ antisymmetric Lamb wave.

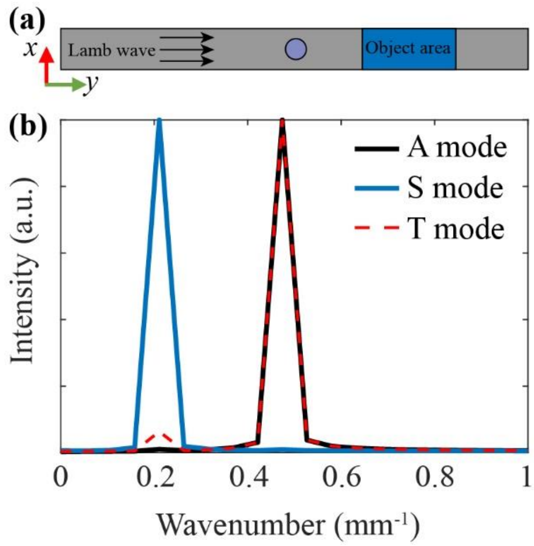

Fig.5. (a): Transmission model (top view). Periodic boundary conditions are applied to the two edges along x directions and perfectly matched layers (not shown) are applied to the two edges along y directions to avoid wave reflection from edges. (b): Wavenumber spectra after FFT for flexural/antisymmetric (A mode) and symmetric (S mode) Lamb incident waves without the pillar and for the transmitted wave (T mode) after the pillars with a flexural incident wave.

Reference

[1] D. Lin, P. Fan, E. Hasman, M.L. Brongersma, Dielectric gradient metasurface optical elements, Science, 345 (2014) 298-302.

[2] N. Yu, P. Genevet, M.A. Kats, F. Aieta, J.P. Tetienne, F. Capasso, Z. Gaburro, Light Propagation with Phase Discontinuities: Generalized Laws of Reflection and Refraction, Science, 334 (2011) 333-337.

[3] M. Khorasaninejad, W.T. Chen, R.C. Devlin, J. Oh, A.Y. Zhu, F. Capasso, Metalenses at visible wavelengths: Diffraction-limited focusing and subwavelength resolution imaging, Science, 352 (2016) 1190-1194.

[4] A.V. Kildishev, A. Boltasseva, V.M. Shalaev, Planar Photonics with Metasurfaces, Science, 339 (2013) 1232009-1232009.

[5] N. Yu, F. Capasso, Flat optics with designer metasurfaces, Nature Materials, 13 (2014) 139-150.

[6] S. Chen, S. Jin, R. Gordon, Subdiffraction Focusing Enabled by a Fano Resonance, Physical Review X, 4 (2014).

[7] L. Zhang, X.Q. Chen, S. Liu, Q. Zhang, J. Zhao, J.Y. Dai, G.D. Bai, X. Wan, Q. Cheng, G. Castaldi, V. Galdi, T.J. Cui, Space-time-coding digital metasurfaces, Nature Communications, 9 (2018) 4334.

[8] S.B. Glybovski, S.A. Tretyakov, P.A. Belov, Y.S. Kivshar, C.R. Simovski, Metasurfaces: From microwaves to visible, Physics Reports, 634 (2016) 1-72.

[9] K. Tang, C. Qiu, M. Ke, J. Lu, Y. Ye, Z. Liu, Anomalous refraction of airborne sound through ultrathin metasurfaces, Scientific Reports, 4 (2015) 6517.

[10] Y. Li, B. Liang, Z.-M. Gu, X.-Y. Zou, J.-C. Cheng, Reflected wavefront manipulation based on ultrathin planar acoustic metasurfaces, Scientific Reports, 3 (2013).

[11] X. Jiang, Y. Li, D. Ta, W. Wang, Ultrasonic sharp autofocusing with acoustic metasurface, Physical Review B, 102 (2020).

[12] Y. Jin, R. Kumar, O. Poncelet, O. Mondain-Monval, T. Brunet, Flat acoustics with soft gradient-index metasurfaces, Nature Communications, 10 (2019).

[13] Y. Xie, W. Wang, H. Chen, A. Konneker, B.-I. Popa, S.A. Cummer, Wavefront modulation and subwavelength diffractive acoustics with an acoustic metasurface, Nature Communications, 5 (2014) 5553.

[14] S. Huang, Z. Zhou, D. Li, T. Liu, X. Wang, J. Zhu, Y. Li, Compact broadband acoustic sink with coherently coupled weak resonances, Science Bulletin, 65 (2020) 373-379.

[15] Y. Jin, X. Fang, Y. Li, D. Torrent, Engineered Diffraction Gratings for Acoustic Cloaking, Physical Review Applied, 11 (2019) 011004.

[16] Y.-X. Shen, Y.-G. Peng, F. Cai, K. Huang, D.-G. Zhao, C.-W. Qiu, H. Zheng, X.-F. Zhu, Ultrasonic super-oscillation wave-packets with an acoustic meta-lens, Nature Communications, 10 (2019).

[17] Y. Shen, X. Zhu, F. Cai, T. Ma, F. Li, X. Xia, Y. Li, C. Wang, H. Zheng, Active Acoustic Metasurface: Complete Elimination of Grating Lobes for High-Quality Ultrasound Focusing and Controllable Steering, Physical Review Applied, 11 (2019).

[18] X. Zhu, K. Li, P. Zhang, J. Zhu, J. Zhang, C. Tian, S. Liu, Implementation of dispersion-free slow acoustic wave propagation and phase engineering with helical-structured metamaterials, Nature Communications, 7 (2016) 11731.

[19] H. Zhu, F. Semperlotti, Anomalous Refraction of Acoustic Guided Waves in Solids with Geometrically Tapered Metasurfaces, Physical Review Letters, 117 (2016).

[20] J. Zhang, X. Su, Y. Pennec, Y. Jing, X. Liu, N. Hu, Wavefront steering of elastic shear vertical waves in solids via a composite-plate-based metasurface, Journal of Applied Physics, 124 (2018) 164505.

[21] Y. Jin, Y. Pennec, B. Bonello, H. Honarvar, L. Dobrzynski, B. Djafari-Rouhani, M.I. Hussein, Physics of surface vibrational resonances: Pillared phononic crystals, metamaterials, and metasurfaces, Reports on Progress in Physics, DOI (2021).

[22] Y. Jin, D. Torrent, Y. Pennec, Y. Pan, B. Djafari-Rouhani, Simultaneous control of the S0 and A0 Lamb modes by graded phononic crystal plates, Journal of Applied Physics, 117 (2015) 244904.

[23] Y. Jin, B. Djafari-Rouhani, D. Torrent, Gradient index phononic crystals and metamaterials, Nanophotonics, 8 (2019) 685.

[24] S.-M. Yuan, A.L. Chen, Y.-S. Wang, Switchable multifunctional fish-bone elastic metasurface for transmitted plate wave modulation, Journal of Sound and Vibration, 470 (2020) 115168.

[25] H. Lee, J.K. Lee, H.M. Seung, Y.Y. Kim, Mass-stiffness substructuring of an elastic metasurface for full transmission beam steering, Journal of the Mechanics and Physics of Solids, 112 (2018) 577-593.

[26] H. Zhu, T.F. Walsh, F. Semperlotti, Total-internal-reflection elastic metasurfaces: Design and application to structural vibration isolation, Applied Physics Letters, 113 (2018) 221903.

[27] M. Zheng, C.I. Park, X. Liu, R. Zhu, G. Hu, Y.Y. Kim, Non-resonant metasurface for broadband elastic wave mode splitting, Applied Physics Letters, 116 (2020) 171903.

[28] J. Rong, W. Ye, Multifunctional elastic metasurface design with topology optimization, Acta Materialia, 185 (2020) 382-399.

[29] J. Rong, W. Ye, S. Zhang, Y. Liu, Frequency-Coded Passive Multifunctional Elastic Metasurfaces, Advanced Functional Materials, 30 (2020) 2005285.

[30] X. Su, Z. Lu, A.N. Norris, Elastic metasurfaces for splitting SV- and P-waves in elastic solids, Journal of Applied Physics, 123 (2017) 091701.

[31] G. Su, Y. Zhang, Y. Liu, T. Wang, Steering Flexural Waves by Amplitude-Shift Elastic Metasurfaces, Journal of Applied Mechanics, 88 (2021).

[32] M.S. Kim, W. Lee, C.I. Park, J.H. Oh, Elastic Wave Energy Entrapment for Reflectionless Metasurface, Physical Review Applied, 13 (2020) 054036.

[33] Y. Liu, Z. Liang, F. Liu, O. Diba, A. Lamb, J. Li, Source Illusion Devices for Flexural Lamb Waves Using Elastic Metasurfaces, Physical Review Letters, 119 (2017) 034301.

[34] Z. Lin, S. Tol, Elastic Metasurfaces for Full Wavefront Control and Low-Frequency Energy Harvesting, Journal of Vibration and Acoustics, 143 (2021).

[35] Y. Ruan, X. Liang, C. Hu, Retroreflection of flexural wave by using elastic metasurface, Journal of Applied Physics, 128 (2020) 045116.

[36] L. Cao, Z. Yang, Y. Xu, Z. Chen, Y. Zhu, S.-W. Fan, K. Donda, B. Vincent, B. Assouar, Pillared elastic metasurface with constructive interference for flexural wave manipulation, Mechanical Systems and Signal Processing, 146 (2021) 107035.

[37] L. Cao, Z. Yang, Y. Xu, S.-W. Fan, Y. Zhu, Z. Chen, B. Vincent, B. Assouar, Disordered Elastic Metasurfaces, Physical Review Applied, 13 (2020) 014054.

[38] Y. Jin, B. Bonello, R.P. Moiseyenko, Y. Pennec, O. Boyko, B. Djafari-Rouhani, Pillar-type acoustic metasurface, Physical Review B, 96 (2017).

[39] Y. Jin, E.I.H. Ei Boudouti, Y. Pennec, B. Djafari-Rouhani, Tunable Fano resonances of Lamb modes in a pillared metasurface, Journal of Physics D: Applied Physics, 50 (2017) 425304.

[40] Y. Jin, Y. Pennec, B. Djafari-Rouhani, Acoustic analogue of electromagnetically induced transparency and Autler–Townes splitting in pillared metasurfaces, Journal of Physics D: Applied Physics, 51 (2018) 494004.

[41] Z. Wen, S. Zeng, D. Wang, Y. Jin, B. Djafari-Rouhani, Robust edge states of subwavelength chiral phononic plates, Extreme Mechanics Letters, 44 (2021) 101209.

[42] L. He, Z. Wen, Y. Jin, D. Torrent, X. Zhuang, T. Rabczuk, Inverse design of topological metaplates for flexural waves with machine learning, Materials & Design, 199 (2021) 109390.

[43] J.-J. Chen, S.-Y. Huo, Z.-G. Geng, H.-B. Huang, X.-F. Zhu, Topological valley transport of plate-mode waves in a homogenous thin plate with periodic stubbed surface, AIP Advances, 7 (2017) 115215.

[44] Y. Jin, W. Wang, A. Khelif, B. Djafari-Rouhani, Elastic Metasurfaces for Deep and Robust Subwavelength Focusing and Imaging, Physical Review Applied, 15 (2021) 024005.

[45] L.W. Schmerr, Fundamentals of Ultrasonic Phased Arrays, Springer International Publishing2014.

[46] X. Jiang, B. Liang, J. Yang, J. Yang, J.-c. Cheng, Acoustic planar antireflective focusing lens with sub-diffraction-limit resolution based on metamaterials, Journal of Applied Physics, 123 (2018) 091717.

[47] B. Graczykowski, The reflection of Rayleigh surface waves from single steps and grooves, Journal of Applied Physics, 112 (2012) 103520.